An Enhanced Feedback Linearization with Fuzzy Logic to Control the Active and Reactive Powers of Bidirectional Three-Phase Grid-Connected Renewable Energy Inverters

Nguyen Gia Minh Thao and Kenko Uchida
Department of Electrical Engineering and Bioscience, Waseda University, Tokyo 169-8555, Japan
Email: {thao, kuchida}@uchi.elec.waseda.ac.jp

***Abstract*—This paper proposes an enhanced feedback linearization method with fuzzy logic (enFBL-FL) to control the active and reactive powers of bidirectional three-phase grid-connected inverters used in renewable energy systems. The proposed control structure is a suitable combination of the direct Feedback Linearization (FBL) and Fuzzy Logic (FL) with newly-added helpful improvements and features. In detail, a unique fuzzy-based scheme is designed to adjust automatically the integral coefficients of the linear control method used in the direct FBL. Its key goals are to increase the response speed, eliminate the overshoot and diminish the steady-state fluctuations in the active and reactive powers. Also, two complementary proportional controllers for the powers are newly added at the outer loop to overcome unexpected errors of the Phase Lock Loop (PLL) and system modeling. In this study, the illustrative inverter utilizes a bidirectional three-level DC-AC converter, an R-L filter and a 250V/10kV 100kVA delta-wye transformer to deliver the total power, obtained from renewable sources and an Energy Storage System (ESS), to the 10kV/60Hz three-phase grid. As well, the inverter can absorb the active power from the grid to charge the ESS as needed. Numerical simulations in MATLAB demonstrate that the suggested enFBL-FL can regulate well the active and reactive powers of the inverter to the reference signals in both negative and positive values, even within large parametric uncertainties in the physical inverter and sudden changes in AC-system load of the grid. Furthermore, comparisons on simulation results, performed separately with the traditional PI control, the direct FBL approach and the newly proposed enFBL-FL, are provided to evaluate salient advantages of the proposed technique.**

***Index Terms*—grid-connected renewable energy inverter, active and reactive power control, harmonics reduction, feedback linearization, fuzzy logic, hybrid control technique**

I. Introduction

In renewable energy systems, to inject effectively the active and reactive powers of DC-AC inverters into the grid, the two powers often can be indirectly controlled by regulating strictly the relevant currents, hence the name *current-controlled* technique [1], [2]. Wherein, the most popular control method, the traditional proportional-integral (PI) control, is often used to regulate the currents. The main advantage of those PI controllers is the simplicity in implementation [3]. However, traditional PI controllers suffer from the slow response speed and large overshoot especially when the reference signals are altered abruptly. Also, the backstepping technique [4], the direct power control (DPC) based on lookup table (LUT) methods [5], [6], and the sliding mode method within the α-β reference frame [7] were applied to control the active and reactive powers of three-phase DC-AC inverters. In our former study [8], a proportional-integral-derivative (PID)-Fuzzy hybrid controller for the single-phase grid-connected photovoltaic (PV) inverters was proposed. In details, fuzzy logic controllers (FLCs) were used to tune online the coefficients (K_P, K_I, K_D) of the PID controller.

In our previous version [1], the PV inverter only can supply the active power to grid (i.e. $P_g \geq 0$); it cannot absorb the active power from the grid. Furthermore, the active power (P_g) and reactive power (Q_g) are indirectly regulated by controlling the corresponding current values (i_{gd}, i_{gq}); if there are some indeterminable errors in the phase lock loop (PLL) module and modeling the inverter, P_g and Q_g may not be guaranteed to track closely the reference signals (P_g^*, Q_g^*) although the current values (i_{gd}, i_{gq}) are controlled to be equal to their desired values (i_{gd}^*, i_{gq}^*). In this case, two complementary direct controllers for the active power (P_g) and reactive power (Q_g) should be implemented at the outer loop to eliminate thoroughly the above drawback. In addition, effects of change in AC-system load have not yet been considered.

In this study, many modifications, improvements and helpful features are newly added as follows. The three-phase transformer is chosen as the delta-wye connection according to the most popular use in grid-connected renewable energy systems; suitable base values used for converting the voltage and current values to per-unit (pu) values can be chosen as line-to-line values as expressed in (1). The newly proposed algorithm, that automatically adjusts the two integral coefficients (K_{d2}, K_{q2}) of the linear control method utilized in the direct FBL, are modified and improved very significantly as shown in

Manuscript received November 30, 2016; revised May 31, 2017.

doi: 10.18178/ijoee.5.1.1-13

Subsection III.B (c.f. [1]). The designed 25-rule FLC is also better optimized, where six association rules are newly changed as described in Table I (c.f. [1]). Two complementary proportional controllers are newly added at the outer loop to ensure the active and reactive powers closely track the reference signals; this helps overcome indeterminable errors in the PLL and system modeling. As well, the way to calculate the mean value is changed to use a discrete integrator module (DIM) for more simplicity in implementation; this module operates as a digital low-pass filter (LPF) and has a good accuracy. These changes are to boost performance and robustness of the proposed control scheme and to add a new feature for the bidirectional inverter. That means the inverter can supply the active power to the grid (i.e. $P_g \geq 0$), and also can absorb the active power from the grid (i.e. $P_g < 0$) to charge the energy storage system (ESS). Moreover, the adaptability of the newly proposed enFBL-FL technique is examined within a case of change in the AC-system load, in which an R-C load is connected suddenly to the 10*kV*/60*Hz* grid (as presented in Subsection IV.C).

II. Modeling of Three-Phase Grid-Connected Inverter Used in Renewable Energy Systems

As shown in Fig. 1, an illustrative bidirectional three-phase grid-tied inverter with a nominal power of 100 *kVA*, connected to Renewable Energy Sources (RES) and battery bank (operates as an ESS), is designed. The total power obtained from RES and ESS is transferred to the three-level voltage source converter (VSC), then synchronously delivered to the 10*kV*/60*Hz* grid via the R-L output filter and the 250*V*/10*kV* delta-wye three-phase transformer. Furthermore, the inverter can be controlled to absorb the active power from the grid to charge the ESS (i.e. $P_g < 0$).

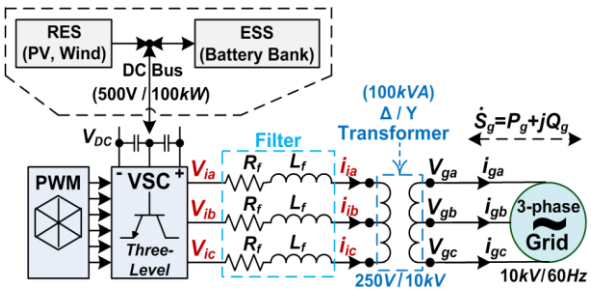

Figure 1. Demonstrative 100kVA grid-connected inverter.

From Fig. 1, the single-phase equivalent circuit of the inverter, with the transformer's impedances referred to the low-voltage winding, is represented in Fig. 2. After that, the simplified equivalent circuit, where the magnetizing branch (n^2R_m, n^2L_m) is neglected, is depicted in Fig. 3.

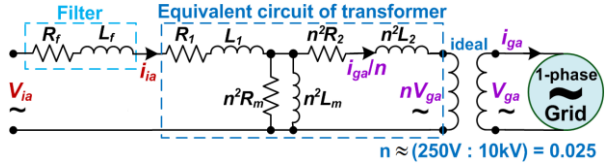

Figure 2. Single-phase equivalent circuit of the inverter.

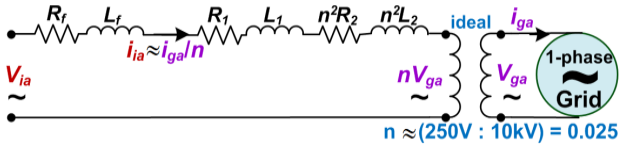

Figure 3. Simplified equivalent circuit after n^2R_m and n^2L_m (in the magnetizing branch) were neglected.

Suitable line-to-line base values used for converting to per-unit (pu) values in this study are chosen as follows.

$$\begin{cases} V_{i,line-to-line}^{(base)} = 250\ V\ ;\ I_{i,line}^{(base)} = 400/\sqrt{3}\ A \\ V_{g,line-to-line}^{(base)} = 10\ kV\ ;\ I_{g,line}^{(base)} = 10/\sqrt{3}\ A \\ Z_i^{(base)} = \dfrac{V_{i,line-to-line}^{(base)}}{\sqrt{3}\ I_{i,line}^{(base)}} = 0.625\ ;\ S_{g,3-phase}^{(base)} = 100\ kVA \end{cases} \quad (1)$$

From (1), per-unit values of the voltages, currents, resistance and inductance in Fig. 3 are computed by (2).

$$\begin{cases} v_{ia}^{(pu)} = \dfrac{v_{ia}}{V_{i,line-to-line}^{(base)}}\ ;\ v_{ga}^{(pu)} = \dfrac{v_{ga}}{V_{g,line-to-line}^{(base)}} = \dfrac{(nv_{ga})}{V_{i,line-to-line}^{(base)}} \\ i_{ia}^{(pu)} = \dfrac{i_{ia}}{I_{i,line}^{(base)}} = \left(i_{ga}/n\right)\dfrac{1}{I_{i,line}^{(base)}} = \dfrac{i_{ga}}{I_{g,line}^{(base)}} = i_{ga}^{(pu)} \\ R_T^{(pu)} = \dfrac{R_T}{Z_i^{(base)}}\ ;\ L_T^{(pu)} = \dfrac{2\pi f_{fuda} \times L_T}{Z_i^{(base)}} = \dfrac{120\pi \times L_T}{Z_i^{(base)}} \end{cases} \quad (2)$$

where: $R_T = R_f + R_1 + n^2R_2$; $L_T = L_f + L_1 + n^2L_2$.

The three-phase active and reactive powers injected into the grid ($P_g^{(pu)}, Q_g^{(pu)}$) are calculated by (3).

$$\begin{bmatrix} P_g^{(pu)} \\ Q_g^{(pu)} \end{bmatrix} = \frac{3}{2}\begin{bmatrix} v_{gd}^{(pu)} & v_{gq}^{(pu)} \\ v_{gq}^{(pu)} & -v_{gd}^{(pu)} \end{bmatrix}\begin{bmatrix} i_{gd}^{(pu)} \\ i_{gq}^{(pu)} \end{bmatrix} \quad (3)$$

where:

$$P_g^{(pu)} = \frac{P_g}{S_{g,3-phase}^{(base)}} = \frac{P_g}{10^5}\ ;\ Q_g^{(pu)} = \frac{Q_g}{S_{g,3-phase}^{(base)}} = \frac{Q_g}{10^5} \quad (4)$$

From (3), if the grid is in normal operation, i.e. $\left[v_{gd}^{(pu)}\right]^2 + \left[v_{gq}^{(pu)}\right]^2 \neq 0$, the currents are computed as

$$\begin{bmatrix} i_{gd}^{(pu)} \\ i_{gq}^{(pu)} \end{bmatrix} = \left(\frac{3}{2}\begin{bmatrix} v_{gd}^{(pu)} & v_{gq}^{(pu)} \\ v_{gq}^{(pu)} & -v_{gd}^{(pu)} \end{bmatrix}\right)^{-1}\begin{bmatrix} P_g^{(pu)} \\ Q_g^{(pu)} \end{bmatrix} \quad (5)$$

From (5) and [1], the differential equations of grid current can be expressed within the state model as shown in (6).

$$\begin{cases} \dot{x} = F(x) + G(x)u \\ y = H(x) \end{cases} \quad (6)$$

where:

- $x = \begin{bmatrix} i_{gd}^{(pu)} & i_{gq}^{(pu)} \end{bmatrix}^T$: are the state variables.
- $u = \begin{bmatrix} v_{id}^{(pu)} & v_{iq}^{(pu)} \end{bmatrix}^T$: are the input control signals.

- $$F(x)=\begin{bmatrix} -\frac{R_T^{(pu)}}{L_T^{(pu)}} i_{gd}^{(pu)} + \omega_g i_{gq}^{(pu)} - \frac{v_{gd}^{(pu)}}{L_T^{(pu)}} \\ -\frac{R_T^{(pu)}}{L_T^{(pu)}} i_{gq}^{(pu)} - \omega_g i_{gd}^{(pu)} - \frac{v_{gq}^{(pu)}}{L_T^{(pu)}} \end{bmatrix}$$
- $$G(x)=\begin{bmatrix} 1/L_T^{(pu)} & 0 \\ 0 & 1/L_T^{(pu)} \end{bmatrix}; H(x)=x=\begin{bmatrix} i_{gd}^{(pu)} & i_{gq}^{(pu)} \end{bmatrix}^T$$

III. The Proposed enFBL-FL Control Technique

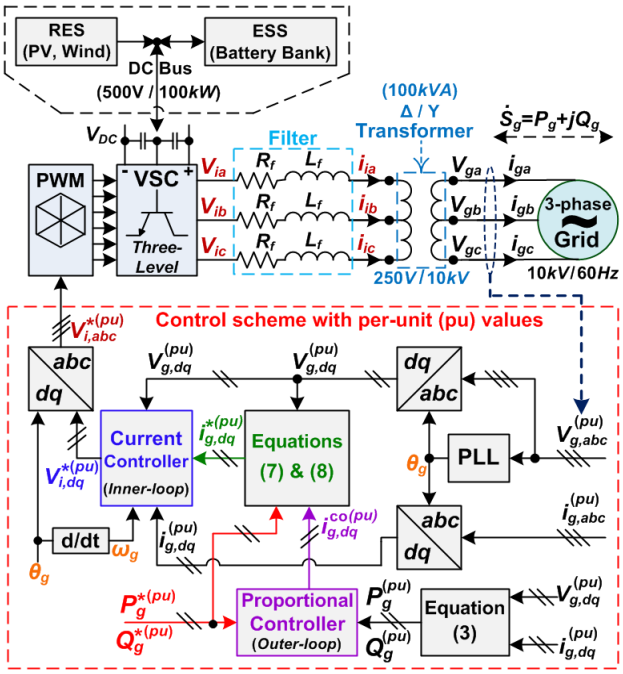

(a) Structure expressed in design and implementation.

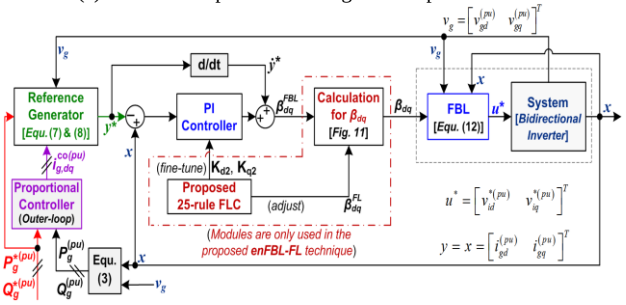

(b) The design structure in (a) re-expressed in control-engineering viewpoint.

Figure 4. The newly proposed enFBL-FL technique.

The design structure of the proposed enFBL-FL technique for the illustrative grid-connected inverter is described in Fig. 4(a). In which, measured values of the grid voltage and current are expressed in the rotating *d-q* reference frame to simplify the design of controllers. θ_g is the instantaneous phase angle of the grid voltage, and detected by the Phase Lock Loop (PLL) module [2], [3]. To simplify the design of controllers, the initial value of θ_g is often chosen as $\theta_g(t=0)=0\,rad$. The newly proposed enFBL-FL scheme is based on per-unit values of the relevant parameters, and it has two control loops. The inner loop is control of the grid currents $i_{g,dq}^{(pu)}$ with the reference signals $i_{g,dq}^{*(pu)}$; this is the main control loop activated in whole operational time. Meanwhile, the outer loop is regulation of the powers $(P_g^{(pu)}, Q_g^{(pu)})$ with the desired values $(P_g^{*(pu)}, Q_g^{*(pu)})$; this is the complementary control loop activated only at the steady state. In detail,

- Initially, as presented in (7), the preliminary desired values of grid current $i_{g,dq}^{m(pu)}$ are computed from the reference values of the active and reactive powers $(P_g^{*(pu)}, Q_g^{*(pu)})$ and the measured actual values of grid voltage $(v_{g,dq}^{(pu)})$. It is noted that (7) and (8) are used as the reference generator module in Fig. 4(b).

$$\begin{cases} i_{gd}^{m(pu)} = \dfrac{2}{3\left(\left[v_{gd}^{(pu)}\right]^2+\left[v_{gq}^{(pu)}\right]^2\right)}\left[v_{gd}^{(pu)}P_g^{*(pu)}+v_{gq}^{(pu)}Q_g^{*(pu)}\right] \\ i_{gq}^{m(pu)} = \dfrac{2}{3\left(\left[v_{gd}^{(pu)}\right]^2+\left[v_{gq}^{(pu)}\right]^2\right)}\left[v_{gq}^{(pu)}P_g^{*(pu)}-v_{gd}^{(pu)}Q_g^{*(pu)}\right] \end{cases} \quad (7)$$

$$\begin{cases} i_{gd}^{*(pu)} = i_{gd}^{m(pu)} - \left[\delta(e_d^M, e_q^M) \times i_{gd}^{co(pu)}\right] \\ i_{gq}^{*(pu)} = i_{gq}^{m(pu)} + \left[\delta(e_d^M, e_q^M) \times i_{gq}^{co(pu)}\right] \end{cases} \quad (8)$$

where $i_{gd}^{co(pu)}$ and $i_{gq}^{co(pu)}$ are computed in Fig. 5; the detailed structure of the DIM is depicted in Fig. 6.

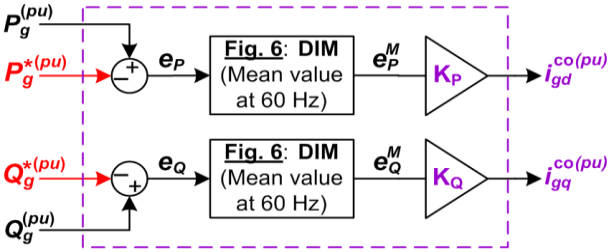

Figure 5. The two proportional controllers used for the active and reactive powers at the outer loop in Fig. 4(b).

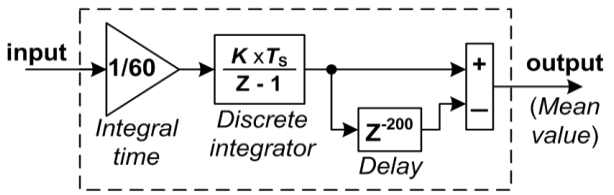

Figure 6. The DIM (K = 2500; $T_S = T_{S\_control}$ = 100 μs) operates as a LPF to calculate the mean value at 60 *Hz*.

Also, two complementary proportional controllers for the active and reactive powers have been added at the outer loop to thoroughly overcome negative effects caused by the indeterminable errors of PLL and system modeling. As represented in (8) and (17), these two proportional controllers are only activated at the steady state, where $\delta(e_d^M, e_q^M)=1$; in contrast, they are

deactivated in the transient state, where $\delta(e_d^M, e_q^M) = 0$. This is to ensure the actual powers to be strictly equal to the desired values.

- After that, from the desired values $i_{g,dq}^{*(pu)}$ calculated in (8) and the measured values of grid voltage and current ($v_{g,dq}^{(pu)}$, $i_{g,dq}^{(pu)}$), the inner-loop Current Controller defines the input control signals $v_{i,dq}^{*(pu)}$. Finally, using the *d-q* to *a-b-c* transformation module, the actual reference signals for the PWM generator of VSC ($v_{i,abc}^{*(pu)}$) are generated.

A. The Direct FBL Control Approach

To force the actual grid currents $i_{g,dq}^{(pu)}$ to track closely their references $i_{g,dq}^{*(pu)}$, the virtual-control signals (β_d, β_q) can be chosen with the linear proportional-integral method as expressed by (9). Wherein, the integrators are necessary to regulate the errors of grid current (e_d, e_q) to be zero and enhance robustness of the control system.

$$\begin{bmatrix}\beta_d\\ \beta_q\end{bmatrix} = \begin{bmatrix}\dot{y}_1\\ \dot{y}_2\end{bmatrix} = \begin{bmatrix}\dot{y}_1^* - K_{d1}e_d - K_{d2}\int e_d dt\\ \dot{y}_2^* - K_{q1}e_q - K_{q2}\int e_q dt\end{bmatrix} \quad (9)$$

where:
$$\begin{cases} e_d = y_1 - y_1^* = i_{gd}^{(pu)} - i_{gd}^{*(pu)} \\ e_q = y_2 - y_2^* = i_{gq}^{(pu)} - i_{gq}^{*(pu)} \end{cases} \quad (10)$$

and $K_{d1}, K_{d2}, K_{q1}, K_{q2}$ are fixed positive values.

From (6), according to the FBL method presented in [1], [9]-[14], the input control signals are computed as

$$u^* = \begin{bmatrix} v_{id}^{*(pu)} \\ v_{iq}^{*(pu)} \end{bmatrix} = G^{-1}(x)\left(-F(x) + \begin{bmatrix}\beta_d\\ \beta_q\end{bmatrix}\right) \quad (11)$$

Substitute $G(x)$, $H(x)$ from (6), and β_d, β_q from (9) into (11), the input control signals are calculated as

$$\begin{cases} v_{id}^{*(pu)} = R_T^{(pu)} i_{gd}^{(pu)} - \omega_g L_T^{(pu)} i_{gq}^{(pu)} + v_{gd}^{(pu)} + L_T^{(pu)}\beta_d \\ v_{iq}^{*(pu)} = R_T^{(pu)} i_{gq}^{(pu)} + \omega_g L_T^{(pu)} i_{gd}^{(pu)} + v_{gq}^{(pu)} + L_T^{(pu)}\beta_q \end{cases} \quad (12)$$

The detailed analysis and the proof on stability of the direct FBL approach can be found in [1].

B. The Newly Proposed enFBL-FL Hybrid Technique

As given in Section II, some physical parameters of the power system, such as R_m, L_m and internal resistors of semiconductor switches in VSC, were neglected in the modeling process. Moreover, in parametric uncertainties, design values of the parameters (R_T, L_T) in Fig. 3 and (6) maybe not equal to their actual values. As shown in (9), because the four coefficients of the linear method for making the virtual-control signals in the FBL approach, $K_{d1}, K_{d2}, K_{q1}, K_{q2}$, are fixed values, modeling errors may cause the errors of grid current (e_d and e_q) to be much larger than zero. As an obvious consequence, those occurring errors (e_d, e_q) will cause big overshoot and steady-state oscillations in the active and reactive powers.

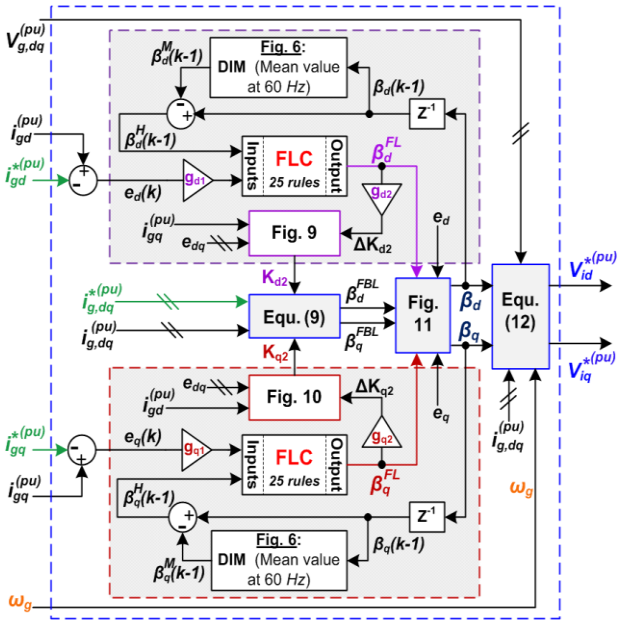

Figure 7. Particular structure of the proposed enFBL-FL technique in the Current Controller module (inner-loop).

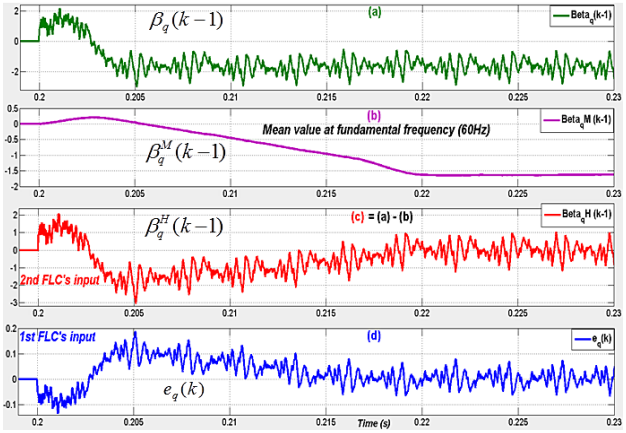

Figure 8. Characteristics of the two inputs of the FLC.

To overcome thoroughly this issue, a unique FLC is designed to enhance efficacy of the linear method applied in the direct FBL for generating the newly compatible final-virtual-control signals (β_d, β_q) as given in Fig. 7. The proposed FLC is designed with two inputs and one output. In detail, the first FLC's input ($e_d(k)$ or $e_q(k)$) is the error between the measured value of grid current and its reference signal; g_{d1} or g_{q1} seen in Fig. 7 is the input scaling factor. The other input, $\beta_d^H(k-1)$ or $\beta_q^H(k-1)$, is the subtraction between the previous final-virtual-control signal ($\beta_d(k-1)$ or $\beta_q(k-1)$) and its mean value at the fundamental frequency of 60 *Hz* ($\beta_d^M(k-1)$ or $\beta_q^M(k-1)$). The characteristics of these values are depicted in (13) and Fig. 8. As presented in parts (c)-(d) of Fig. 8, if $\beta_q^H(k-1)$ increases, $e_q(k)$ will decrease; and vice versa. Similarly, impact of $\beta_d^H(k-1)$ on $e_d(k)$

is exactly the same as the effect of $\beta_q^H(k-1)$ on $e_q(k)$. The above relationship between the two FLC's inputs is the key idea to develop fuzzy membership functions and association rules. The values (β_d^{FBL} and β_q^{FBL}) in Fig. 7 denote for the signals (β_d and β_q, respectively) in (9).

$$\begin{cases} \beta_d^H(k-1) = \beta_d(k-1) - \beta_d^M(k-1) \\ \beta_q^H(k-1) = \beta_q(k-1) - \beta_q^M(k-1) \end{cases} \quad (13)$$

where $\beta_d^M(k-1)$ and $\beta_q^M(k-1)$ are the two output values from DIM (as shown in Fig. 6) with the two input values $\beta_d(k-1)$ and $\beta_q(k-1)$, respectively.

As shown in Fig. 7, the FLC's output, $\beta_d^{FL}(k)$ or $\beta_q^{FL}(k)$, used for two separate functions as follows.

1) The first function of the proposed 25-rule FLC

That is to tune automatically the coefficients (K_{d2}, K_{q2}) of the integral modules in the linear method used in the direct FBL as shown in Fig. 7. K_{d2} and K_{q2} in (9) now are changeable values and are adjusted suitably in the transient state by the designed FLC as expressed in Figs. 9 and 10, respectively. Obviously, its key objective is to boost the response speed and eliminate efficiently the overshoot of the two powers in the transient state, especially when the desired values ($P_g^{*(pu)}, Q_g^{*(pu)}$) are changed suddenly. Then, K_{d2} and K_{q2} will be maintained at the suitable fixed values at the steady state to enhance stability of the proposed enFBL-FL technique.

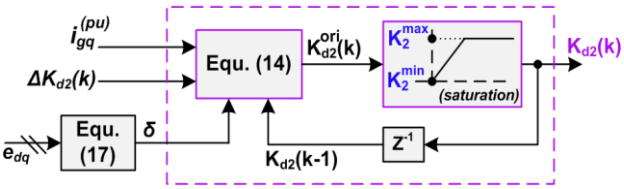

Figure 9. Tuning automatically the coefficient $K_{d2}(k)$.

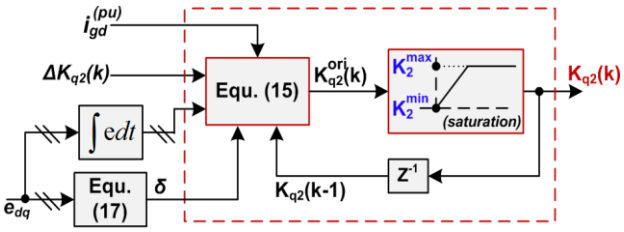

Figure 10. Tuning automatically the coefficient $K_{q2}(k)$.

$$K_{d2}^{ori}(k) = K_{d2}(k-1) + \left[1 - \delta(e_d^M, e_q^M)\right] \mathrm{sgn}\left(-i_{gq}^{(pu)}\right) \Delta K_{d2}(k) \quad (14)$$

where $\Delta K_{d2}(k) = g_{d2}\beta_d^{FL}(k)$ as described in Fig. 7. The initial value of $K_{d2}(k)$ is $K_{d2}(0) = K_2^{min} > 0$.

$$K_{q2}^{ori}(k) = \begin{cases} K_{q2}(k-1) + \left[1 - \delta(e_d^M, e_q^M)\right] \mathrm{sgn}\left(i_{gd}^{(pu)}\right) \Delta K_{q2}(k); & \text{if } \int e_q \geq 0 \\ K_{q2}(k-1) + \left[1 - \delta(e_d^M, e_q^M)\right] \mathrm{sgn}\left(i_{gd}^{(pu)} \times \left(-\int e_d\right)\right) \Delta K_{q2}(k); & \text{else} \end{cases} \quad (15)$$

where $\Delta K_{q2}(k) = g_{q2}\beta_q^{FL}(k)$ as shown in Fig. 7. And the initial value of $K_{q2}(k)$ is $K_{q2}(0) = K_2^{min} > 0$.

In (14) and (15), sgn is the sign function defined as given by (16); and $\delta(e_d^M, e_q^M)$ is the value to determine the present operation state of the power system, which is the transient or steady state, as expressed in (17).

$$\mathrm{sgn}(z) = \begin{cases} 1 \ ; \text{if } z > 0 \\ 0 \ ; \text{if } z = 0 \\ -1 \ ; \text{if } z < 0 \end{cases} \quad (16)$$

$$\delta(e_d^M, e_q^M) = \begin{cases} 1; \text{if } \begin{cases} \left|e_d^M(k)\right| \leq \varepsilon = 0.6\% << 1\ pu \\ \left|e_q^M(k)\right| \leq \varepsilon = 0.6\% << 1\ pu \end{cases} \text{(at steady state)} \\ 0; \text{otherwise (system is in the transient state)} \end{cases} \quad (17)$$

where e_d^M and e_q^M are the output values from DIM (seen in Fig. 6) with the input values e_d and e_q, respectively.

In power systems, the measured value of grid current consists of the component at the fundamental frequency and the harmonic values. Thus, at the steady state, when the two powers are regulated closely to the references, the mean values of the errors of grid current at the fundamental frequency (e_d^M, e_q^M) become so small (nearly zero); this means that $\left|e_{d,q}^M\right| \to \varepsilon \ll 1\ pu$. Normally, in order to satisfy well control qualities, the steady-state error should be regulated to be smaller than 6% of the reference value. The operation value of desired signal is often used with 10-100% of its nominal value ($\pm 1\ pu$); this means the absolute value of reference signal is usually in the interval [0.1 pu 1 pu]. So the limit value ε can be chosen as 6% × 0.1 pu = 0.6% pu, which seems small enough to be utilized for almost operation cases.

In this study, as shown in (16) and (17), where ε is chosen as 0.6% pu, the power system will be in the transient state if $\delta(e_d^M, e_q^M) = 0$, or at the steady state if $\delta(e_d^M, e_q^M) = 1$. According to the value $\left[1 - (e_d^M, e_q^M)\right]$ as expressed in (14) and (15), the first function of FLC's output is only activated in the transient state when $\delta(e_d^M, e_q^M) = 0$. It means the two coefficients (K_{d2}, K_{q2}) are changeable values in the transient state to improve the transient dynamics; and then, they are fixed values at the steady state to ensure stability of the proposed method.

Interpretation for variables of sgn in (14) and (15): In the first equation of (12), since the reactance value $\omega_g L_T^{(pu)}$ is often much larger than the resistance value $R_T^{(pu)}$, and $v_{gd}^{(pu)}$ normally is a DC fixed quantity [1]-[3], so $v_{id}^{*(pu)}$ is mostly dependent on the changes of $-i_{gq}^{(pu)}$ and β_d. Therefore, to eliminate thoroughly the impact of $-i_{gq}^{(pu)}$ on $v_{id}^{*(pu)}$, the change of β_d must be contra with the variation of $-i_{gq}^{(pu)}$. On the other hand, in the first equation of (9), the alteration of β_d is also in opposition to the variation of $K_{d2}\int e_d dt$. Furthermore, in this study, because the active power $P_g^{(pu)}$ is controlled only with non-negative value within the range of [0 pu 1 pu], the grid current $i_{gd}^{(pu)}$ has value in the range [0 pu, 1 pu]. As a consequence, the modification of K_{d2} should be driven in the same direction of the variation of $-i_{gq}^{(pu)}$. After

checking carefully with simulation results in this study, to tune K_{d2} appropriately, the parameter variable in the sgn function in (14) should be chosen as $-i_{gq}^{(pu)}$.

Similarly, from the second formulas in (9) and (12), the change of K_{q2} should be in the same direction of the variation of $i_{gd}^{(pu)}$. Hence, to adjust K_{q2} properly, the parameter variable in the sgn function in the upper part of (15) should be selected as $i_{gd}^{(pu)}$ in the case where $\int e_q \geq 0$. Because the reactive power $Q_g^{(pu)}$ is controlled with both negative and positive values in the range of [-1 *pu*, 1 *pu*], the grid current $i_{gq}^{(pu)}$ has value in the range of [-1 *pu*, 1 *pu*]; therefore, the integral value $\int e_q$ in (15) may change suddenly its sign (negative/positive) in some special circumstances. Also, according to the opposite signs between the values $\omega_g L_T^{(pu)} i_{gd}^{(pu)}$ and $-\omega_g L_T^{(pu)} i_{gq}^{(pu)}$ in (12) and checking the simulation results, the additional consideration on the integral value $-\int e_d$ in (15) is necessary in tuning K_{q2} where $\int e_q < 0$. As a result, to adjust K_{q2} suitably in this case where $\int e_q < 0$, parameter variables in the sgn functions should be chosen with both $i_{gd}^{(pu)}$ and $-\int e_d$ as shown in the lower part of (15).

2) The second function of the proposed 25-rule FLC

As shown in Figs. 7 and 11, the FLC's output value $(\beta_d^{FL}, \beta_q^{FL})$ is also used to complement properly for the final-virtual-control signal (β_d, β_q) in order to reduce efficiently fluctuations in the powers at the steady state. Additionally, to avoid unexpected negative impacts on transient responses of the powers, this function should be activated only when the inverter operates in the steady state. As given by (17), the controlled power system will be at the steady state if $\delta(e_d^M, e_q^M) = 1$. So, conversely with the first function that is only activated in the transient state when $\delta(e_d^M, e_q^M) = 0$, the second function of FLC's output is only activated at the steady state when $\delta(e_d^M, e_q^M) = 1$ as described in Fig. 11 and (18).

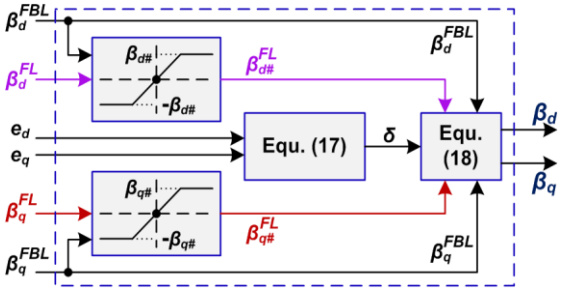

Figure 11. The detailed structure of the second function of the proposed FLC's output.

$$\begin{bmatrix} \beta_d(k) \\ \beta_q(k) \end{bmatrix} = \begin{bmatrix} \beta_d^{FBL}(k) \\ \beta_q^{FBL}(k) \end{bmatrix} + \delta(e_d^M, e_q^M) \begin{bmatrix} \beta_{d\#}^{FL}(k) \\ \beta_{q\#}^{FL}(k) \end{bmatrix} \quad (18)$$

As shown in Fig. 11, the two values $\beta_{d\#}^{FL}$ and $\beta_{q\#}^{FL}$ are respectively the output signals of β_d^{FL} and β_q^{FL} after the two saturation modules. In generating the final-virtual-control signals (β_d, β_q) in (18), the output two values of (9) in Fig. 7, β_d^{FBL} and β_q^{FBL}, are the major components; meanwhile, $\beta_{d\#}^{FL}$ and $\beta_{q\#}^{FL}$ are complementary quantities for β_d^{FBL} and β_q^{FBL}, respectively. In this study and [1], after checking simulation results, the suitable limits can be chosen as 25% of $|\beta_d^{FBL}|$ or $|\beta_q^{FBL}|$ as given below.

$$\begin{cases} \beta_{d\#}(k) = 0.25 \times |\beta_d^{FBL}(k)| \\ \beta_{q\#}(k) = 0.25 \times |\beta_q^{FBL}(k)| \end{cases} \quad (19)$$

As a result, the second function of FLC's output is used as an output filter for the virtual-control signals (β_d, β_q) in the steady state. In detail, its objective is to shape the signal forms of β_d and β_q to be smoother. This will help diminish the harmonic distortions of grid current in order to lower efficiently oscillations in the powers, especially in parametric uncertainty conditions.

Two inputs: have five linguistic variables, membership function, and value in the interval of [-1 1].

- $e_d(k)$ or $e_q(k)$ = {Negative Large, Negative Small, Zero, Positive Small, Positive Large} = {NL, NS, ZE, PS, PL}
- $\beta_d^H(k-1)$ or $\beta_q^H(k-1)$ = {Negative Large, Negative Small, Zero, Positive Small, Positive Large} = {NL, NS, ZE, PS, PL}

The two inputs of the proposed FLC $(e_d(k), \beta_d^H(k-1))$ have both negative and positive values, soo the number of linguistic variables for each FLC's input $(N_{variable})$ should be an odd value to can divide into three groups as negative linguistic variables, 'zero' variable and positive linguistic variables. Obviously, the value of $N_{variable}$ cannot be 1 due to the very bad control quality. Moreover, if the value of $N_{variable}$ is 3, linguistic variables of each FLC's input will have one negative value, 'zero' value and one positive value; this clearly cannot perform a good control quality owing to the little number of control cases. Besides, as shown in Fig. 7, the proposed enFBL-FL technique utilizes two FLCs; thus, if the value of $N_{variable}$ is chosen as 7, the total computation time of two FLCs may become pretty long. As a result, the value of $N_{variable}$ should be chosen as 5, which is the most suitable value on considering between the control quality and total computation time.

Output: has seven linguistic variables and value in the interval of [-1 1].

$\beta_d^{FL}(k)$ or $\beta_q^{FL}(k)$ = {Negative Large, Negative Medium, Negative Small, Zero, Positive Small, Positive Medium, Positive Large} = {NL, NM, NS, ZE, PS, PM, PL}

Membership functions: The membership functions of the two inputs and output are depicted in Figs. 12 and 13, respectively.

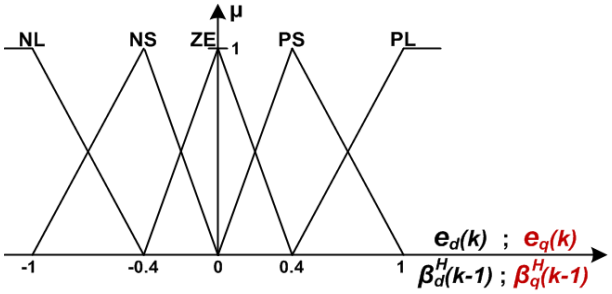

Figure 12. Membership functions for two FLC's inputs.

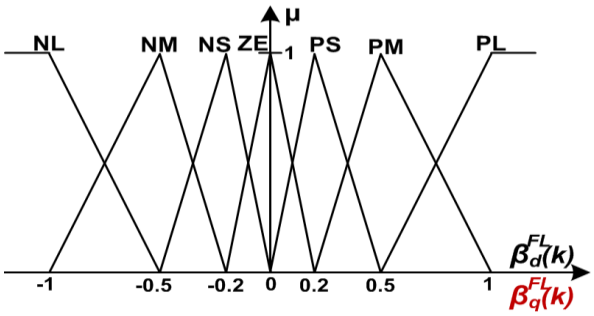

Figure 13. Membership functions for the FLC's output.

Fuzzy association rules: The fuzzy associative matrix is described in Table I. It has totally 5 × 5 = 25 rules, and each rule is expressed in the form "**if**…**then**…". The fuzzy rules are developed and optimized according to the authors' logical deduction from observing impacts of the second FLC's input on the first FLC's input as depicted in the parts (c)-(d) of Fig. 8.

TABLE I. FUZZY ASSOCIATION RULES OF THE PROPOSED FLC

$\beta_d^{FL}(k)$ or $\beta_q^{FL}(k)$		$\beta_d^H(k-1)$ or $\beta_q^H(k-1)$				
		NL	NS	ZE	PS	PL
$e_d(k)$ or $e_q(k)$	NL	NS	NM	NL	NL	NL
	NS	PS	ZE	NS	NM	NL
	ZE	PM	PS	ZE	NS	NM
	PS	PL	PM	PS	ZE	NS
	PL	PL	PL	PL	PM	PS

Furthermore, as compared with the previous version [1], the designed 25-rule FLC is better optimized in this research, where six association rules are newly modified as follows: "**if** $e_q(k)$ is NL and $\beta_q^H(k-1)$ is NL **then** $\beta_q^{FL}(k)$ is NS"; "**if** $e_q(k)$ is NL and $\beta_q^H(k-1)$ is NS **then** $\beta_q^{FL}(k)$ is NM"; "**if** $e_q(k)$ is NL and $\beta_q^H(k-1)$ is ZE **then** $\beta_q^{FL}(k)$ is NL"; "**if** $e_q(k)$ is PL and $\beta_q^H(k-1)$ is ZE **then** $\beta_q^{FL}(k)$ is PL"; "**if** $e_q(k)$ is PL and $\beta_q^H(k-1)$ is PS **then** $\beta_q^{FL}(k)$ is PM"; "**if** $e_q(k)$ is PL and $\beta_q^H(k-1)$ is PL **then** $\beta_q^{FL}(k)$ is PS". The purpose of the changes is to boost significantly the response speed as a high priority when the error value ($e_d(k)$ or $e_q(k)$) is far away its desired value of 0. The deductive way to interpret other association rules in Table I can be found in [1] and [15].

Program in MATLAB for analysis on stability: The detailed analysis and proof on stability of the proposed enFBL-FL control technique can be found in [1], [16], [17]; where the process in analyzing stability is performed with *LMI Control Toolbox* of MATLAB [18]. In this study, specific values for the five parameters manually chosen for analysis are shown in (20) and (21).

$$K_1^{\min} = 15\ ;\quad K_1^{\max} = 16 \tag{20}$$

$$\begin{cases} K_2^{\min} = T_{s\_control} = 10^{-4}\ ;\quad K_2^{\max} = 1 \\ \Delta K_2^{\max} = \left| g_{d2}\beta_d^{FL} \right|_{\max} = 0.2 \times T_{s\_control} = 0.2 \times 10^{-4} \end{cases} \tag{21}$$

As shown in (21), $\Delta K_2^{max} = 0.2 \times 10^{-4}$; therefore, according to Fig. 9 and (14), $K_{d2}(k)$ will be a slowly-varying positive parameter in the transient state. The MATLAB program used for analysis on stability with the specified parameter values in (20)-(21) is as follows.

```
A0 = ltisys([0 1; 0 0])          %  A0
A1 = ltisys([0 0; 0 -1], 0)      %  A1 (for K-d1)
A2 = ltisys([0 0; -1 0], 0)      %  A2 (for K-d2)

pv = pvec('box', [15 16; 1e-4 1], [0 0; -0.2e-4 0.2e-4])

ps = psys(pv,[A0 A1 A2])   % Affine parameter-dependent model

tmin = quadstab(ps)   % command "quadstab": Quadratic Stability

[tmin_2,P0,P1,P2] = pdlstab(ps) % command "pdlstab": Parameter-Dependent-Lyapunov Stability
```

Then, results of the above program are obtained as below.

```
This system is quadratically stable
 tmin =  -5.8116e-04      % Negative value shows the system is stable
  ...
 This system is stable for the specified parameter trajectories

 tmin_2 = -0.0012   % Negative value shows the control system is stable

 P0 =        % The symmetric matrix P0 (details in [1])
    1.0e+03 *
      4.0276   -0.0019
     -0.0019    0.0301

 P1 =        % The symmetric matrix P1 (details in [1])
    330.4938    0.7575
      0.7575   -12.4014

 P2 =        % The symmetric matrix P2 (details in [1])
     54.6665   -271.0764
   -271.0764    21.6456
```

IV. NUMERICAL SIMULATION RESULTS

The power system is simulated with Fuzzy Logic and SimPowerSystems toolboxes of MATLAB [1], [19], and

in discrete time with two different sampling times. Namely, the first one used for the detailed simulation model and measurement is T_{S_power} = 1 μs; and the other used for generating control signals is $T_{S\_control}$ = 100 μs. In addition, the traditional PI controllers given in Fig. 14 are used to implement into the Current Controller in Fig. 4(a) for evaluation purpose. Detailed parameters of the designed inverter and controllers are shown in Table II.

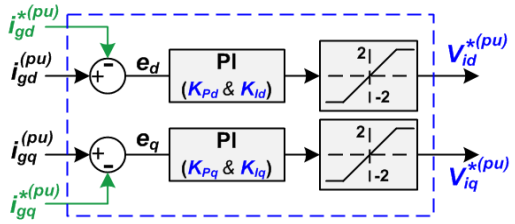

Figure 14. Traditional PI controllers [1], [2] implemented into the Current Controller in Fig. 4(a).

TABLE II. PARAMETERS OF THE INVERTER AND THREE CONTROLLERS

Physical Module	**Parameter and Value**
R-L output filter	R_f = 2 $m\Omega$; L_f = 250 μH
Per-phase parameters of the transformer (*Fig. 2*)	R_1 = 0.001 pu ; L_1 = 0.03 pu R_2 = 0.001 pu ; L_2 = 0.03 pu R_m = 500 pu ; L_m = 500 pu
Control scheme	**Parameter and Value**
The traditional PI control (*Fig. 14*)	$K_{Pd} = K_{Pq}$ = 0.5 ; $K_{Id} = K_{Iq}$ = 20
The direct FBL in (9)	$K_{d1} = K_{q1}$ = 16 ; $K_{d2} = K_{q2}$ = 0.25
The newly proposed enFBL-FL (*Figs. 4, 5 and 7*)	K_P = 2.5 ; K_Q = 1 $K_{d1} = K_{q1}$ = 16 ; $g_{d1} = g_{q1}$ = 4; $g_{d2} = g_{q2} = 0.2 \times T_{s\_control}$

The inverter starts to run at the time t = 0.2 s; the reference values of the active and reactive powers (with *Case 1* and *Case* 2) are altered according to the step functions in four operational periods as follows.

- First period: from the time t = 0.2 s to t = 0.35 s,
  $P_g^{*(pu)}$ = 0.8 pu and $Q_g^{*(pu)}$ = 0 pu
- Second period: from the time t = 0.35 s to t = 0.5 s,
  $P_g^{*(pu)}$ = 0.8 pu and $Q_g^{*(pu)}$ = -0.6 pu
- Third period: from the time t = 0.5 s to t = 0.65 s,
  $P_g^{*(pu)}$ = -0.4 pu and $Q_g^{*(pu)}$ = -0.6 pu
- Fourth period: from the time t = 0.65 s to t = 0.8 s,
  $P_g^{*(pu)}$ = -0.4 pu and $Q_g^{*(pu)}$ = 0.6 pu.

where the actual values (P_g^*, Q_g^*) can be computed by (4). It is noted that, in the third and fourth operational periods, because $P_g^{*(pu)}$ = -0.4 pu, the inverter is controlled to absorb the active power from the grid to charge the ESS.

A. *Case 1: Without the Parametric Uncertainties*

As seen in Fig. 15, the performance of the traditional PI control has the little fluctuations in the two powers; nevertheless, it includes the large overshoots and very slow response. Whereas, the direct FBL method shows fast response and fairly small oscillations in the powers at the steady state as described in Fig. 16. However, it produces quite large overshoots at the step changes of the two reference signals at t = 0.2 s and at t = 0.65 s. Finally, Fig. 17 represents that the proposed enFBL-FL not only inherits the main advantage of the direct FBL approach in terms of rapid response, but also eliminates significantly the overshoots in the transient state (especially when the reference signals are changed at t = 0.2 s and t = 0.65 s) and decreases the steady-state fluctuations in the powers.

Detailed operations of two functions of the designed FLC in the enFBL-FL technique are illustrated in Fig. 18. In detail, according to the first FLC's function represented in Figs. 9 and 10, the coefficients K_{d2}, K_{q2} now are tuned automatically and suitably in the transient state, and then they are kept at the fixed values at the steady state, as described in the upper part of Fig. 18. In fact, this assists to eliminate the large overshoot in the transient state. Besides, impacts of the second FLC's function on the virtual-control signals (β_d, β_q) are presented in the lower part of Fig. 18. The shapes of the two signals β_d and β_q become smoother when the second FLC's function is activated (to be ON) at the steady state. This helps reduce noticeably the harmonic distortion of grid current.

TABLE III. THD OF THE GRID CURRENT IN *CASE 1*

Control scheme	**THD of grid current (%)**	
	From t = 0.3 s to t = 0.35s	From t = 0.45 s to t = 0.5 s
The PI control	4.34 %	3.32 %
The direct FBL	4.86 %	3.86 %
The newly proposed enFBL-FL	4.35 %	3.41 %

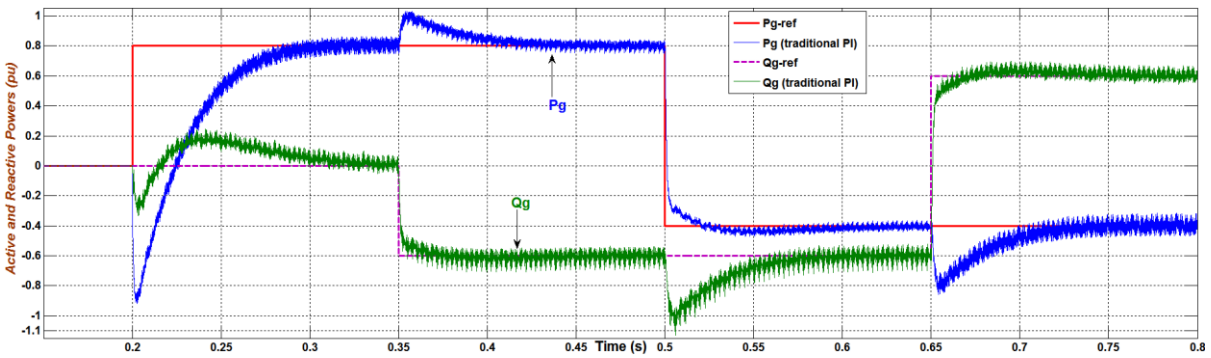

Figure 15. The performance with the traditional PI control, Case 1.

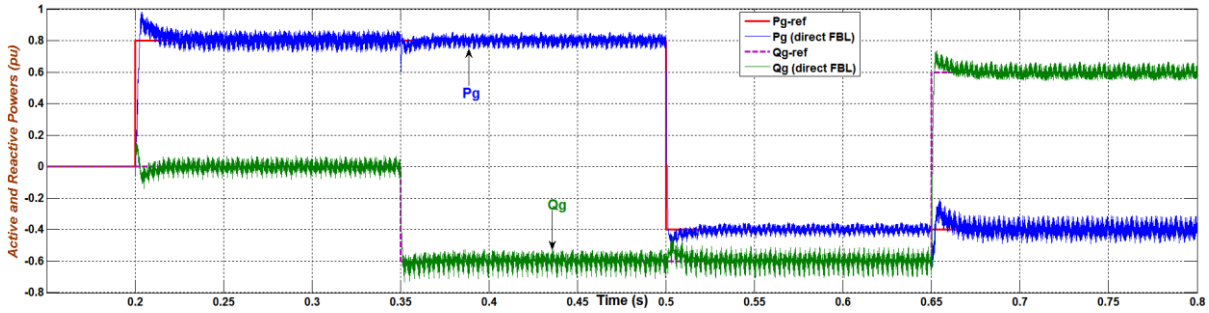

Figure 16. The performance with the direct FBL approach, Case 1.

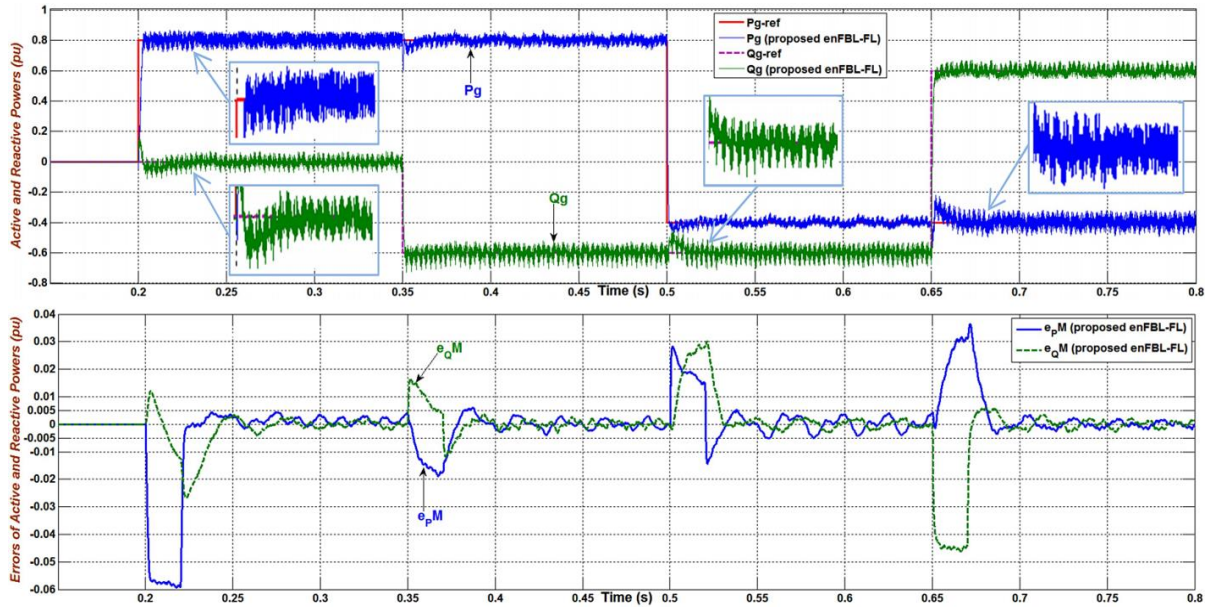

Figure 17. The performance with the newly proposed enFBL-FL hybrid technique, Case 1.

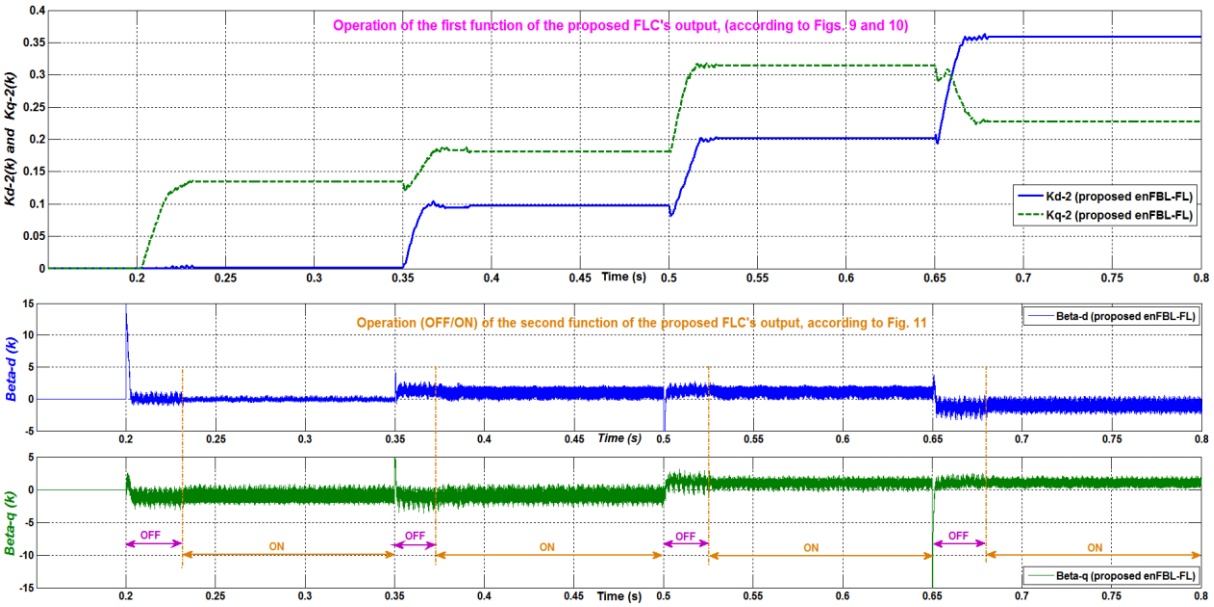

Figure 18. Operations of two functions of the FLC in the newly proposed enFBL-FL technique, Case 1.

In addition, Table III shows the total harmonic distortion (THD) of grid current measured at the steady state in two periods: from the time t = 0.3 s to t = 0.35 s, and from t = 0.45 s to t = 0.5 s. In the results attained with the proposed enFBL-FL, as compared to the direct FBL, the second FLC's function aided to lower THD from 4.86% to 4.35%, and from 3.86 % to 3.41 %, respectively. THD values with the suggested enFBL-FL are equivalent to the ones obtained from the traditional PI control.

B. Case 2: Within the Parametric Uncertainties

In this situation, the actual values of the parameters in Fig. 2, R_f, R_1, R_2, L_f, L_1 and L_2, now are smaller of 30% as compared to their original values in Table II.

As described in Figs. 19-22, because of the big parametric uncertainties, power ripples presently are pretty much larger than the prior responses in *Case 1*. As seen in Fig. 19, the performance of the traditional PI control still includes the large overshoots and very slow response. Whereas, the direct FBL method has the quick response and fairly big oscillations at the steady state in the powers as described in Fig. 20; its performance still contains the pretty large overshoots especially when the desired values are changed significantly at t = 0.2 s and t = 0.65 s. Lastly, Fig. 21 represents that the proposed enFBL-FL technique not only has the rapid response but also decreases markedly the overshoots in the transient state (especially when the reference values are varied considerably at t = 0.2 s and t = 0.65 s), and maintains the steady-state oscillations be equivalent as in the PI control.

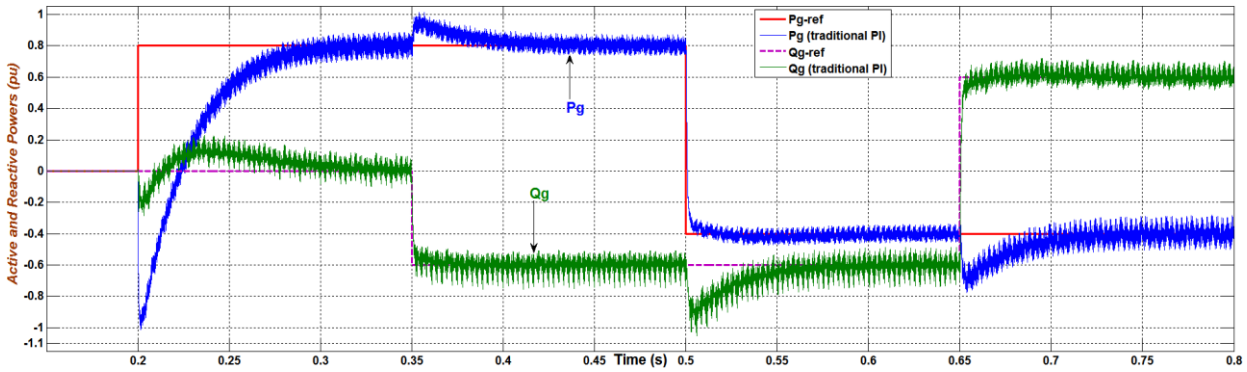

Figure 19. The performance with the traditional PI control, Case 2.

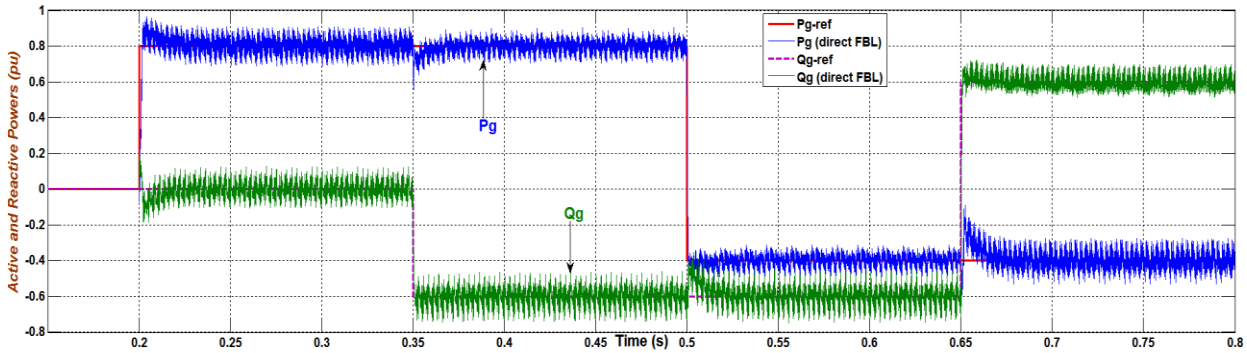

Figure 20. The performance with the direct FBL approach, Case 2.

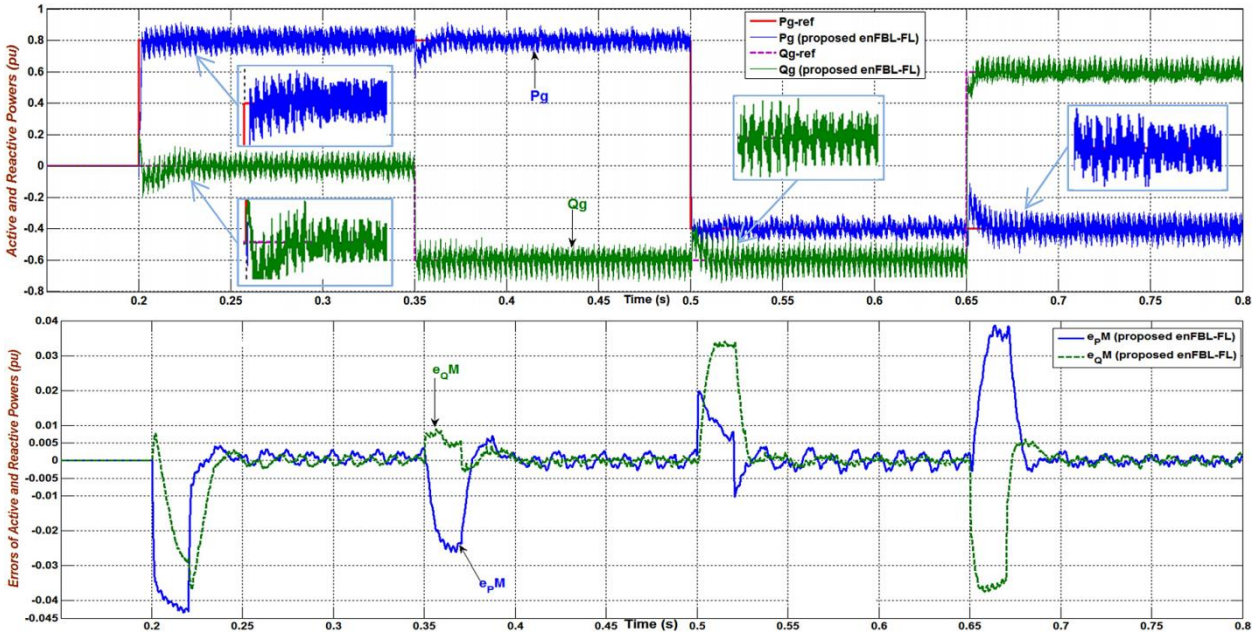

Figure 21. The performance with the newly proposed enFBL-FL hybrid technique, Case 2.

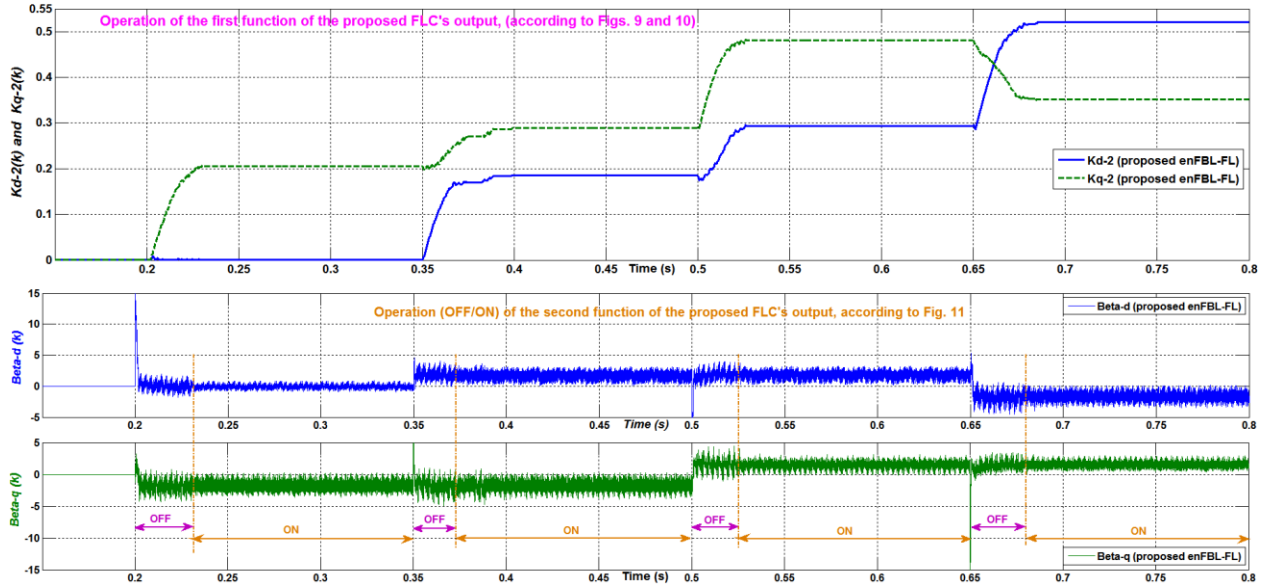

Figure 22. Operations of two functions of the FLC in the newly proposed enFBL-FL technique, Case 2.

TABLE IV. THD OF THE GRID CURRENT IN *CASE 2*

Control scheme	THD of grid current (%)	
	From t = 0.3 s to t = 0.35s	From t = 0.45 s to t = 0.5 s
The PI control	6.44 %	5.01 %
The direct FBL	7.55 %	6.08 %
The newly proposed enFBL-FL	6.40 %	5.06 %

In both *Case 1* and *Case 2*, the mean values (at the fundamental frequency of 60 *Hz*) of errors of the powers are stabilized closely to be tiny (nearly zero) as described in the lower parts of Figs. 17 and 21, respectively. The two functions of the 25-rule FLC in the newly suggested enFBL-FL technique still perform properly as presented in Fig. 22. Furthermore, Table IV shows the THD values of grid current measured at the steady state in the first two operational periods. In the results with the proposed enFBL-FL, as compared with the direct FBL, the second FLC's function helped to reduce significantly THD values from 7.55% to 6.40%, and from 6.08% to 5.06%, respectively. Also, the THD values with the proposed enFBL-FL are tantamount to the ones from the PI control.

C. *Case 3: Within the Sudden Change of AC Load*

In this case, the desired values of active and reactive powers are altered according to step functions as follows.

- From the time t = 0.2 s to t = 0.3 s :
  $P_g^{*(pu)}$= 0.8 pu and $Q_g^{*(pu)}$= 0 pu
- From the time t = 0.3 s to t = 0.5 s :
  $P_g^{*(pu)}$= 0.8 pu and $Q_g^{*(pu)}$= -0.6 pu
- At the time t = 0.4 s, an R-C load is connected unexpectedly to the 10kV/60Hz three-phase grid.

With the results obtained in *Case 1* and *Case 2*, the newly proposed enFBL-FL hybrid technique has better performance than the traditional PI control and the direct FBL approach. This third case is performed to evaluate adaptability of the proposed enFBL-FL within the sudden change of the AC-system load in the grid. Responses of the controlled system are illustrated in Figs. 23 and 24.

When the R-C load is connected suddenly to the grid at the time of t = 0.4 s, the phase angles of the grid currents (i_{ga}, i_{gb}, i_{gc}) are changed noticeably; it obviously causes the large fluctuations in the active and reactive powers of the inverter in the transient state for the period of [0.4 s, 0.435 s], as depicted in the upper part of Fig. 23. The coefficients (K_{d2}, K_{q2}) in the suggested enFBL-FL technique are adjusted automatically and appropriately (as presented in the upper part of Fig. 24) to reduce the transient-state fluctuations quickly; as a result, the two powers are stabilized well after the time of t = 0.435 s. The mean values (at the fundamental frequency) of errors of the powers are regulated closely to be nearly zero as illustrated by the lower part of Fig. 23. Also, as given in the lower part of Fig. 24, the second function of the FLC in the proposed enFBL-FL still operates properly to help diminish the steady-state oscillations in the two powers.

In all the cases, the suitable combination of the inner-loop current control (see Figs. 4 and 7) and the outer-loop power regulation (see Figs. 4 and 5) clearly has enhanced noticeably the effectiveness, adaptability and robustness of the newly proposed enFBL-FL hybrid technique.

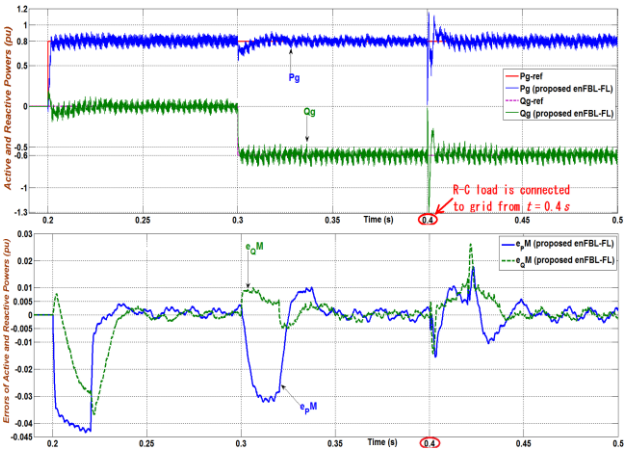

Figure 23. Performance with the enFBL-FL, Case 3.

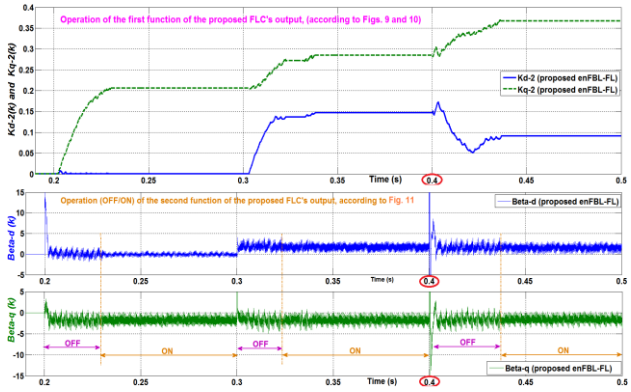

Figure 24. Operations of two functions of FLC, Case 3.

V. Discussion

This paper has introduced the enhanced FBL-based hybrid technique with fuzzy logic, namely enFBL-FL, to regulate the active and reactive powers of bidirectional three-phase grid-connected inverters used in renewable energy systems. In which, the 25-rule FLC is improved better to boost efficacy of the linear proportional-integral method utilized in the direct FBL approach, details:

- As the first function, the FLC tunes automatically and fittingly the coefficients (K_{d2}, K_{q2}) of integral modules in the linear method. This helped enhance substantially the transient response (response speed, overshoot) of the two powers, especially when the reference signals are changed remarkably and suddenly. This function is only activated in the transient state and deactivated at the steady state.
- Moreover, as the second function, the 25-rule FLC adjusts appropriately the final virtual-control signals (β_d, β_q) to diminish the steady-state oscillations in the two powers, especially in parametric uncertainty conditions. This function is only activated at the steady state and deactivated in the transient state.

Also, two complementary proportional controllers for the active and reactive powers have been added at the outer loop to thoroughly overcome the negative effects caused by the indeterminable errors of PLL and system modeling. These proportional controllers are only activated at the steady state and deactivated in the transient state; this assists to ensure the actual powers to be strictly equal to their desired values. As a new operational function, the inverter can be controlled to absorb the active power from the grid (i.e. $P_g < 0$) to charge the ESS when required.

VI. Conclusion

Within the designed $100\,kVA$ bidirectional three-phase grid-connected inverter, simulations in MATLAB have demonstrated the proposed enFBL-FL technique can regulate very well the active and reactive powers to the desired signals. As compared to the traditional PI control and the direct FBL, the proposed enFBL-FL has much better performance in boosting the response speed and reducing the overshoot of the powers. Also, the steady-state oscillation in the powers with the proposed enFBL-FL is kept in an acceptable range, which is equivalent to the one with the traditional PI control. Furthermore, the suggested enFBL-FL is highly robust against parametric variations and sudden change in the AC-system load.

In summary, for the proposed enFBL-FL, fuzzy logic has helped enhance efficacy of the direct FBL approach in order to efficiently inherit the main advantages of both the direct FBL (such as the quick response speed and high robustness) and the traditional PI control (such as small steady-state fluctuation and acceptable THD value), as well as to eliminate drawbacks of the direct FBL (such as the fairly large overshoot and steady-state fluctuation).

In our next work, a decentralized control strategy for grid-connected large-scale renewable energy farms combined with many residential houses will be studied and developed. Each local agent in a renewable-energy farm will consist of a nominal power of around 100 kW plus a battery bank to supply power directly to a group of several houses. With this strategy, crucial problems on the power quality and optimization of economic benefits for users in houses will be examined comprehensively.

Acknowledgment

This work was supported by JST-CREST Grant Number JPMJCR15K2, Japan.

References

[1] N. G. M. Thao and K. Uchida, "Active and reactive power control techniques based on feedback linearization and fuzzy logic for three-phase grid-connected photovoltaic inverters," *Asian Journal of Control*, vol. 17, no. 5, pp. 1522-1546, Sep. 2015.

[2] M. P. Kazmierkowski and L. Malesani, "Current control techniques for three-phase voltage-source pwm converters: A survey," *IEEE Transactions on Industrial Electronics*, vol. 45, no. 5, pp. 691-703, October 1998.

[3] G. A. Raducu, "Control of grid side inverter in a B2B configuration for WT applications," Master Thesis, Aalborg University, June 2008.

[4] M. Benchagra, M. Hilal, Y. Errami, M. Maaroufi, and M. Ouassaid, "Nonlinear control of DC-bus voltage and power for voltage source inverter," *Proceedings of ICMCS*, pp. 1049-1054, October 2012.

[5] T. Noguchi, H. Tomiki, S. Kondo, and I. Takahashi, "Direct power control of PWM converter without power source voltage sensors," *IEEE Transactions on Industry Applications*, vol. 34, no. 3, pp. 473-479, May/June 1998.

[6] D. Zhi, L. Xu, and B. W. Williams, "Improved direct power control of grid-connected DC/AC converters," *IEEE Trans. on Power Electronics*, vol. 24, no. 5, pp. 1280-1292, May 2009.

[7] J. Hu, L. Shang, Y. He, and Z. Q. Zhu, "Direct active and reactive power regulation of grid-connected DC/AC converters using sliding mode control approach," *IEEE Transactions on Power Electronics*, vol. 26, no. 1, pp. 210-222, January 2011.

[8] N. G. M. Thao, M. T. Dat, T. C. Binh, and N. H. Phuc, "PID-Fuzzy logic hybrid controller for grid-connected photovoltaic inverters," *Proceedings of 5th IFOST*, pp. 140-144, October 2010.

[9] D. E. Kim and D. C. Lee, "Feedback linearization control of grid-interactive PWM converters with LCL filters," *Journal of Power Electronics*, vol. 9, no. 2, pp. 288-299, March 2009.

[10] X. Bao, F. Zhuo, Y. Tian, and P. Tan, "simplified feedback linearization control of three-phase photovoltaic inverter with an LCL filter," *IEEE Transactions on Power Electronics*, vol. 28, no. 6, pp. 2739-2752, June 2013.

[11] X. Zhou, Y. B. Guo, M. Zhang, X. Zhang, and H. Chen, "Dual feedback linearization control of three-phase pulse-width-

modulation voltage source rectifier based on direct power control," *Proceedings of 7th IPEMC*, pp. 1859-1865, June 2012.
[12] T. L. Chien, C. C. Chen, Y. C. Chen, and S. L. Wu, "Improved fuzzy feedback linearization and sinswat-transformation control of inverted pendulum," *Control and Cybernetics*, vol. 39, no. 4, pp. 1069-1093, July/August 2010.
[13] R. Marino and P. Tomei, *Nonlinear Control Design: Geometric, Adaptive, and Robust*, 1st ed., Prentice Hall, August 1995.
[14] N. G. M. Thao and K. Uchida, "Control the active and reactive powers of three-phase grid-connected photovoltaic inverters using feedback linearization and fuzzy logic," *Proceedings of the 3rd Australian Control Conference*, pp. 133-140, November 2013.
[15] T. J. Ross, *Fuzzy Logic with Engineering Applications*, 3rd ed., Wiley, March 2010.
[16] P. Gahinet, P. Apkarian, and M. Chilali, "Affine parameter-dependent lyapunov functions and real parametric uncertainty," *IEEE Transactions on Automatic Control*, vol. 41, no. 3, pp. 436-442, March 1996.
[17] C. Scherer, "Robust stability," in *Course of Linear Matrix Inequalities in Control*, Delft University of Technology, 2009.
[18] P. Gahinet, A. Nemirovski, A. J. Laub, and M. Chilali, "LMI control toolbox for use with MATLAB," in *User's Guide*, version 1, The MathWorks, Inc., May 1995.
[19] P. Giroux, G. Sybille, C. Osorio, and S. Chandrachood, "Two demonstrations of a grid-connected PV array using SimPowerSystems," in *File Exchange - MATLAB Central*, The MathWorks, Inc., October 2012.

Nguyen Gia Minh Thao obtained B.Eng. (honors) and M.Eng. (research) degrees in Electrical and Electronics Engineering from Ho Chi Minh City University of Technology (HCMUT), Vietnam, in March 2009 and 2011, respectively. He obtained a Dr. Eng. degree in Electrical Engineering from Waseda University, Japan, in 2015. In April 2009, he became a probationary lecturer in the Faculty of Electrical and Electronics Engineering at HCMUT, where he has been a Lecturer. He is currently a postdoctoral Research Associate at Waseda University, Japan. His research interests include nonlinear control, intelligent control, renewable energy systems and power network optimization. He is a member of the Society of Instrument and Control Engineers (SICE) and Asian Control Association (ACA).

Kenko Uchida received B.S., M.S., and Dr. Eng. degrees in Electrical Engineering from Waseda University, Japan, in 1971, 1973, and 1976, respectively. He is currently a Professor in the Department of Electrical Engineering and Bioscience at Waseda University. His research interests are robust/optimization control and control problems in energy systems and biology. He is a member of SICE, ACA, the Institute of Electrical Engineers of Japan, and the Institute of Electrical and Electronics Engineers (IEEE).